

OPERATION and PROPOSALS

1. Outline of the Accelerators

Two electron storage rings, the PF ring and the PF-AR, have been operated as dedicated light sources at the Photon Factory. The PF ring is always operated by a constant current of 450 mA at 2.5 GeV with two operation modes: normal filling mode and hybrid filling mode. The hybrid filling mode has an isolated bunch with a current of 30 mA, and accounts for about 30% of the total user time.

At the PF-AR, about half of the operation time was conducted at a lower energy mode of 5 GeV which was introduced in FY2019. The 5 GeV mode contributes to saving electricity and extending the operation time of the PF-AR. However, there is the unfortunate restriction that simultaneous injection with the PF ring is impos-

sible, and therefore hybrid operation is also impossible for the PF ring when the PF-AR is operating at 5 GeV. This restriction is caused by the need to change the current of a DC bending magnet of the beam transport line to reduce the injection energy of the PF-AR. To overcome the restriction, the bending magnet is switched at an interval of several minutes to perform pseudo top-up operation. We have proposed modifying the configuration of the beam transport line to enable full-time top-up injection.

The machine parameters of the rings and the calculated spectral performances are listed in **Tables 1** and **2**. The spectral distributions of synchrotron radiation (SR) from the bending magnets and the insertion devices are shown in **Fig. 1**.

Table 1: Principal beam parameters of the PF ring and PF-AR.

	PF ring	PF-AR	
Energy	2.5 GeV	6.5 GeV	5 GeV
Natural emittance	34.6 nm rad	290 nm rad	170 nm rad
Circumference	187 m	377 m	←
RF frequency	500.1 MHz	508.6 MHz	←
Bending radius	8.66 m	23.7 m	←
Energy loss per turn	0.4 MeV	6.66 MeV	2.33MeV
Damping time			
Vertical	7.8 ms	2.5 ms	5.4 ms
Longitudinal	3.9 ms	1.2 ms	2.7 ms
Natural bunch length	10 mm	16 mm	15 mm
Momentum compaction factor	0.00644	0.0126	←
Natural chromaticity			
Horizontal	-12.9	-13.6	←
Vertical	-17.3	-13.3	←
Stored current	450 mA	60 mA	←
Normal filling	250 bunches	Single	←
Beam lifetime	20 h (at 450 mA)	14 h (at 50 mA)	7 h (at 50 mA)
Hybrid filling	Single (30 mA) + 131 bunches (420 mA)		
Beam lifetime	8 h (450 mA)		

Table 2: Calculated spectral performances of the bending source and all the insertion devices at the PF ring (2.5 GeV, 450 mA) and PF-AR (6.5 GeV, 60 mA).

Name	E/I GeV/mA	λ_u cm	N	L m	$G_y(G_x)$ cm	$B_y(B_x)$ T	Type of magnet	σ_x mm	σ_y mm	$\sigma_{x'}$ mrad	$\sigma_{y'}$ mrad	$K_y(K_x)$	ϵ_s/ϵ_c keV	D	B	P_T kW
PF																
2.5/450																
Bend								0.41	0.059	0.178	0.012		4	5.38E+13	3.48E+14	
SGU#01		1.2	39	0.5	0.4	0.7	P(NdFeB)	0.6	0.012	0.088	0.029	0.78		4.56E+16	9.90E+17	0.4
U#02-1		6	60	3.6	2.8	0.4	H(NdFeB)	0.65	0.042	0.054	0.008	2.3		2.73E+17	1.55E+18	1.07
U#02-2		16	17	2.72	2.6	0.33(0.33)	P(NdFeB)	0.65	0.042	0.054	0.008	4.93(4.93)		9.53E+15	4.58E+16	0.53
SGU#03		1.8	26	0.5	0.4	1	P(NdFeB)	0.6	0.012	0.088	0.029	1.68		2.50E+16	5.44E+17	0.82
MPW#05-W		12	21	2.5	2.64	1.4	H(NdFeB)	0.71	0.045	0.078	0.009	16	5.9	2.22E+15	1.10E+16	8.83
U#13		7.6	47	3.6	2.3	0.68(0.34)	P(NdFeB)	0.74	0.02	0.094	0.019	4.84(2.42)		6.85E+16	4.70E+17	3.7
VW#14					5	5	S.C.	0.53	0.045	0.128	0.008		20.8	5.42E+13	3.59E+14	
SGU#15		1.76	27	0.5	0.4	0.97	P(NdFeB)	0.6	0.012	0.088	0.029	1.37		4.38E+15	9.44E+16	0.75
U#16-1 & 16-2		5.6	44	2.5	2.1	0.6(0.38)	P(NdFeB)	0.654	0.042	0.055	0.008	3(2)		1.42E+17	7.87E+17	2.2
SGU#17		1.6	29	0.5	0.4	0.92	P(NdFeB)	0.6	0.012	0.088	0.029	1.37		7.88E+15	1.71E+17	0.69
U#19		6.8	55	3.74	2.4	0.71(0.46)	P(NdFeB)	0.71	0.045	0.078	0.009	4.5(2.92)		1.14E+17	5.08E+17	4.76
U#28		16	22	3.52	2.7	0.33(0.33)	P(NdFeB)	0.53	0.045	0.127	0.008	4.93(4.93)		1.39E+16	6.59E+16	1.36
PF-AR																
6.5/60																
Bend								1	0.2	0.593	0.036		26	3.90E+13	3.11E+13	
EMPW#NE01-W		16	21	3.36	3(11)	1(0.2)	P(NdFeB)	1.07	1.07	0.268	0.032	15(3)	28(90%)	1.84E+15	2.54E+15	5.52
U#NE03		4	90	3.6	1	0.8	P(NdFeB)	1.57	0.17	0.312	0.029	3		1.29E+16	7.66E+15	3.708
U#NW02		4	90	3.6	1	0.8	P(NdFeB)	1.57	0.17	0.312	0.029	3		1.29E+16	7.66E+15	3.708
U#NW12		4	95	3.8	1	0.8	P(NdFeB)	1.57	0.17	0.312	0.029	3		1.29E+16	7.66E+15	3.912
U#NW14-36		3.6	79	2.8	1	0.8	P(NdFeB)	1.35	0.14	0.338	0.036	2.8		7.69E+15	6.49E+15	3.12
U#NW14-20		2	75	1.5	0.8	0.63	P(NdFeB)	0.75	0.07	0.383	0.038	1.17		7.69E+15	6.49E+15	0.936

λ_u : period length, M : number of periods, L : length of undulator or wiggler, $G_y(G_x)$: minimum vertical (horizontal) gap height, $B_y(B_x)$: maximum vertical (horizontal) magnetic field, H: hybrid configuration, S.C.: superconducting magnet, σ_x, σ_y : horizontal or vertical beam size, $\sigma_{x'}, \sigma_{y'}$: horizontal or vertical beam divergence, $K_y(K_x)$: vertical (horizontal) deflection parameter, D : photon flux density (photons/sec/mrad²/0.1%b.w.), B : brilliance (photons/sec/mm²/mrad²/0.1%b.w.), P_T : total radiated power. MPW#05 and EMPW#NE01 are operated in wiggler mode denoted by -W.

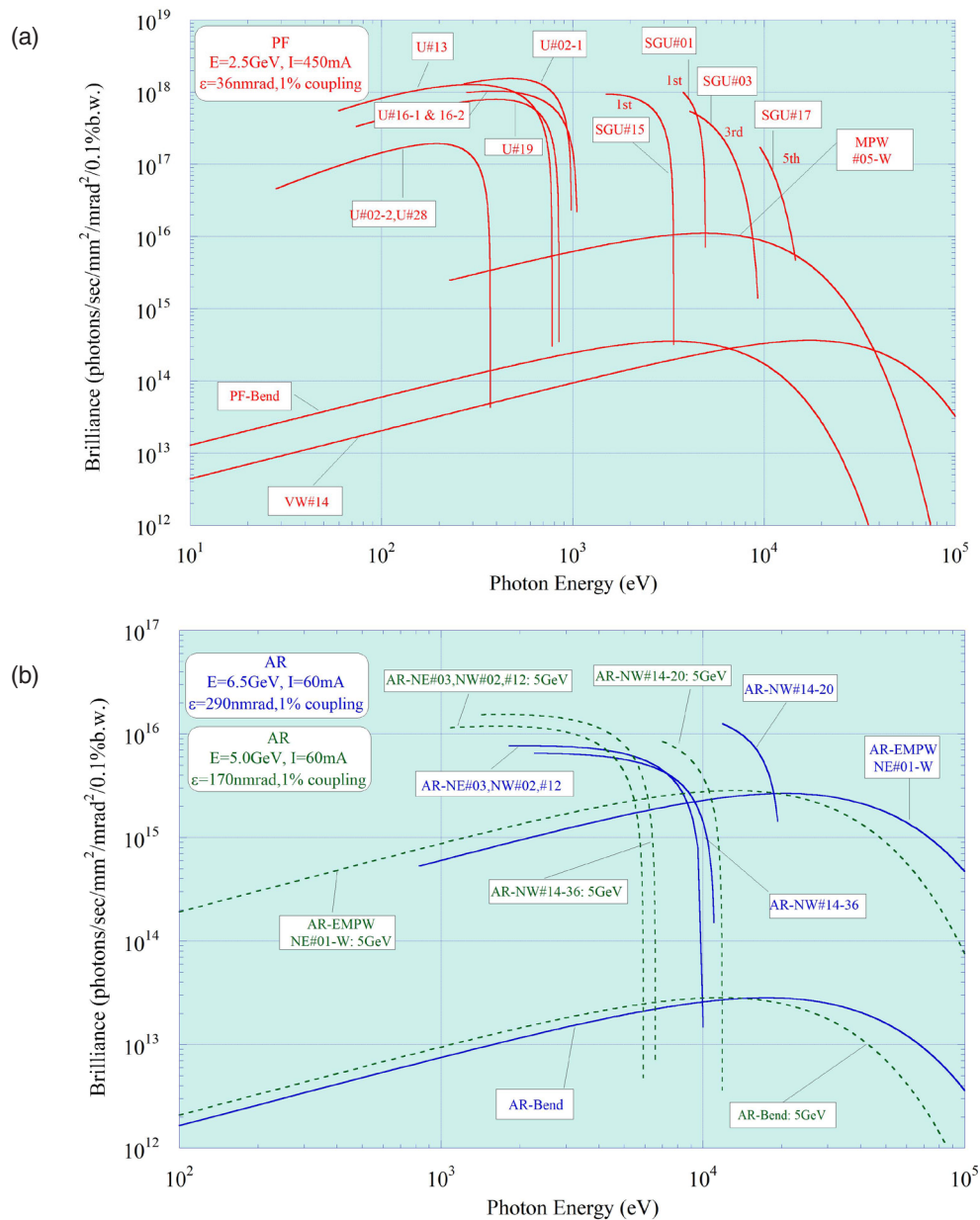


Figure 1: Synchrotron radiation spectra available at the Photon Factory. (a) PF ring, and (b) PF-AR, blue curves for 6.5 GeV and green dashed curves for 5 GeV. The name of each source is listed in **Table 2**. The spectral curve of each undulator is the locus of the peak of the first harmonic within the allowance range of K parameter. For SGU#01 and SGU#15, the first harmonic regions are shown. For SGU#03, the third harmonic region is shown. For SGU#17, the fifth harmonic region is shown.

2. Operation Summary

The operation schedule of the PF ring and the PF-AR in FY2020 is shown in **Fig. 2**. The statistics of the accelerator's operation for the past decade are shown in **Fig. 3**.

For the PF ring, to secure 3,000 hours of user operation time, the total operation time of about 3,500 hours has been maintained for the past few years. To achieve this goal, the first phase of operation had been scheduled to run from May 8 to July 1, 2020. However, in April, a state of emergency was declared for the first time in

Japan due to the spread of Covid-19. In response, the decision was made to cancel the operation from May to July. Later, as the first wave of infections subsided and the state of emergency was lifted nationwide on May 25, only the PF ring was operated for about two weeks in the latter half of June. The superconducting wiggler, which requires a long time to prepare for cooling, was not operated in this June's operation. Meanwhile, the PF-AR was completely shut down from May to July. However, by operating for a longer period than usual in the second and third phases, the resulting operation time was almost the same as in the previous year.

	MON 9 17	TUE 9 17	WED 9 17	THU 9 17	FRI 9 17	SAT 9 17	SUN 9 17	MON 9 17	TUE 9 17	WED 9 17	THU 9 17	FRI 9 17	SAT 9 17	SUN 9 17	MON 9 17	TUE 9 17	WED 9 17	THU 9 17	FRI 9 17	SAT 9 17	SUN 9 17
Date	6.8	9	10	11	12	13	14	15	16	17	18	19	20	21	22	23	24	25	26	27	28
PF																					
AR																					
Date	29	30	7.1	2	3	4	5	6	7	8	9	10	11	12	13	14	15	16	17	18	19
PF																					
AR																					
Date	10.12	13	14	15	16	17	18	19	20	21	22	23	24	25	26	27	28	29	30	31	11.1
PF																					
AR																					
Date	2	3	4	5	6	7	8	9	10	11	12	13	14	15	16	17	18	19	20	21	22
PF																					
AR																					
Date	23	24	25	26	27	28	29	30	31	12.1	2	3	4	5	6	7	8	9	10	11	12
PF																					
AR																					
Date	13	14	15	16	17	18	19	20	21	22	23	24	25	26	27	28	29	30	31		
PF																					
AR																					
Date	2.15	16	17	18	19	20	21	22	23	24	25	26	27	28	3.1	2	3	4	5	6	7
PF																					
AR																					
Date	8	9	10	11	12	13	14	15	16	17	18	19	20	21	22	23	24	25	26	27	28
PF																					
AR																					
Date	29	30	31	4.1	20	21	22	23	24	25	26	27	28	29	30	31	4.1	2	3	4	5
PF																					
AR																					

- PF: PF ring
AR: PF-AR
- Tuning and ring machine study
 - Ring machine study
 - Hybrid Mode Operation
 - Short maintenance and /or machine study
 - Experiment using SR
 - B Bonus
 - 5GeV Operation

Figure 2: Operation schedule of PF ring and PF-AR in FY2020.

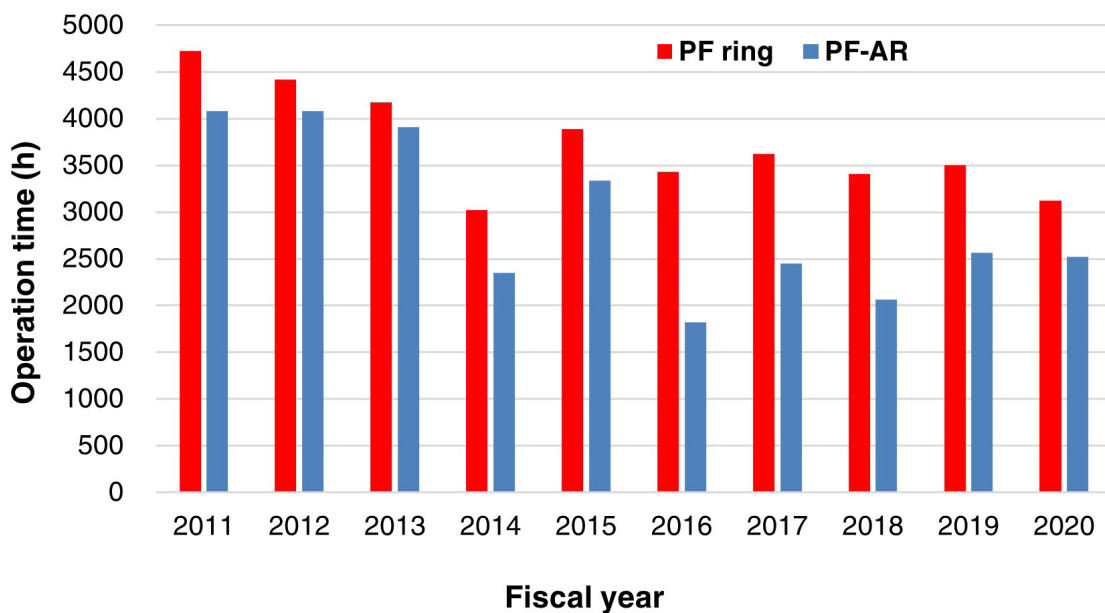


Figure 3: Total operation time for PF ring and PF-AR.

Detailed operation statistics and the number of failures from FY2011 to FY2020 are listed in **Table 3** for the PF ring. A breakdown of the total downtime in FY2020 is shown in **Fig. 4**. In last year's PF Highlights, we corrected the total operating time for FY2018 in **Table 3**, but we failed to correct the values of the failure rate and the MTBF for FY2018. This year, we have also revised those two values.

The total breakdown time for FY2020 was unusually long compared to previous years. This was due to a severe failure of the pulse bending magnet installed at the end of the LINAC disturbing the injection for several days. The failure was caused by a burn-out of the power supply in the early morning of March 26, 2021. The inspection showed that the breakdown could not be quickly repaired.

The user time was scheduled until 9 a.m. on April 1, but the operation was declared over on March 30, and the remaining two days were cancelled. The breakdown time in **Table 3** includes all the time after March 26 when the system was judged to be seriously broken. Therefore, most of the failure time is accounted for by this single failure, and the breakdown of the failure time in Fig. 4 shows that 95.6% is due to the injection failure. The number of failures per year was almost the same

as in previous years, and the MTBF was well over 100 hours, the same as in previous years. Fortunately, the power supply of the pulse bending magnet was able to be repaired within the short shutdown period in April, and there was no delay in the start of the next year's operation.

The accident of a cooling water leak, which occurred in the beamline frontend of BL-12 on December 8, 2020, subsequently triggered the failure of the gap drive mechanism of undulator #13 which was wetted by water. The gap drive mechanism required several months for repair, and it was not possible to adjust the gap and polarization of undulator #13 until the end of March. This failure was also recovered during the short shutdown period in April.

The PF ring has been in operation since 1982, and most of the accelerator components have been upgraded with modifications to achieve low emittance or enhancement of the straight sections. The only things that had not been updated since 1982 were the bodies of the bending magnets and the vacuum ducts of the injection section. In these vacuum ducts, there was a vacuum leak from a cooling water path receiving the synchrotron radiation power, and the operation was continued for several years with insufficient cooling.

Table 3: Operation statistics for the PF ring from FY2011 to FY2020.

Fiscal Year	2011	2012	2013	2014	2015	2016	2017	2018	2019	2020
Total operation time (h)	4728	4416	4176	3024	3888	3432	3624	3408	3504	3120
Scheduled user time (h)	2832	3792	3504	2328	3048	2928	3000	2832	3064	2584
Ratio of user time (%)	59.9	85.9	83.9	77.0	78.4	85.3	82.8	83.1	87.4	82.8
No. of failures	18	23	22	15	23	18	14	17	20	15
Total down time (h)	14.9	37.6	52.1	11.4	14.4	17.3	16.6	28.4	59.9	158.4
Failure rate (%)	0.5	1.0	1.5	0.5	0.5	0.6	0.6	1.0	2.0	6.1
MTBF (h)	157.3	164.9	159.3	155.2	132.5	162.7	214.3	166.6	153.2	172.3
Mean down time (h)	0.8	1.6	2.4	0.8	0.6	1.0	1.2	1.7	3.0	10.6

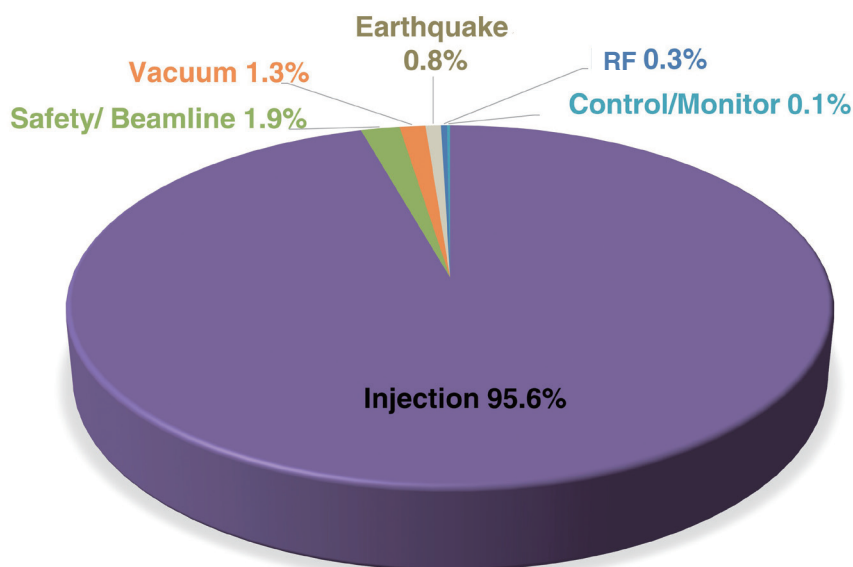


Figure 4: Breakdown of the total down time for the PF ring in FY2020.

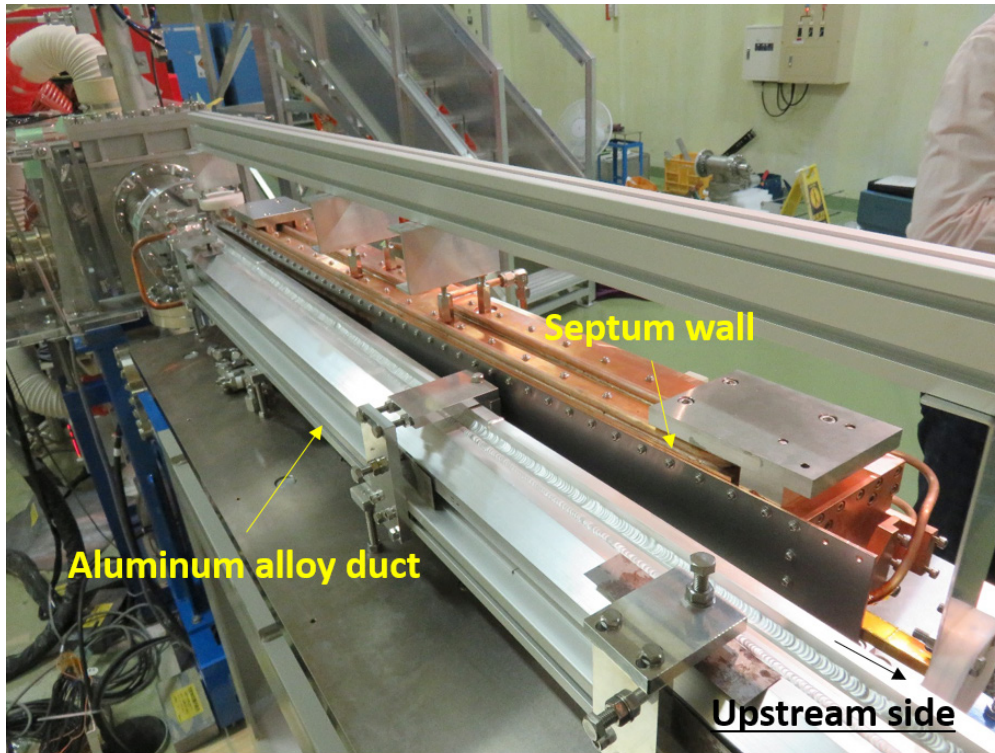


Figure 5: Reconstruction of the injection section of the PF ring. Parameters of the injection point have been improved to enable injection with a smaller horizontal aperture.

Table 4: Operation statistics for PF-AR from FY2011 to FY2020.

Fiscal Year	2011	2012	2013	2014	2015	2016	2017	2018	2019	2020
Total operation time (h)	4080	4080	3912	2352	3336	1821	2448	2064	2568	2520
Scheduled user time (h)	2904	3672	3478	1992	2784	1104	2136	1608	2112	2112
Ratio of user time (%)	71.2	90.0	88.9	84.7	83.5	60.6	87.3	77.9	82.2	83.8
No. of failures	49	33	47	22	18	13	55	25	8	14
Total down time (h)	38.7	29.7	99.6	37	31	18.3	24.7	26.4	12.3	168.1
Failure rate (%)	1.3	0.8	2.9	1.9	1.1	1.7	1.2	1.6	0.6	8
MTBF (h)	59.3	111.3	74.0	90.5	154.7	84.9	38.8	64.3	264.0	150.9
Mean down time (h)	0.8	0.9	2.1	1.7	1.7	1.4	0.4	1.1	1.5	12

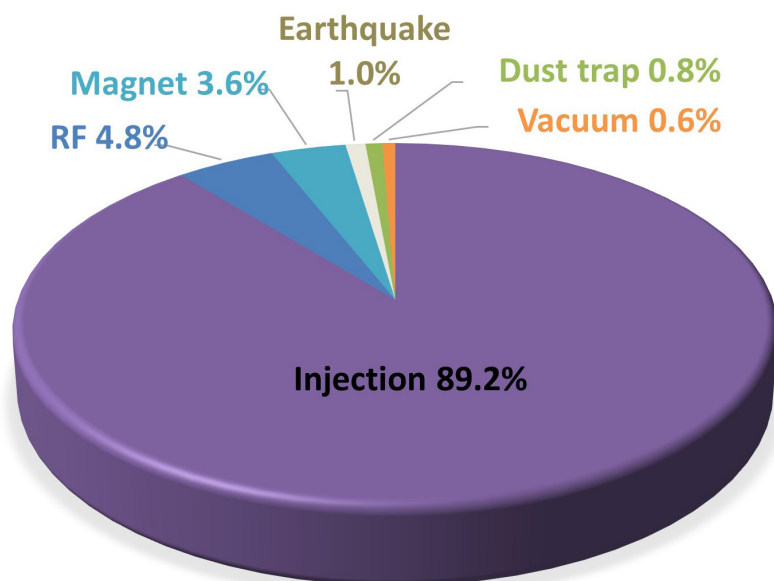


Figure 6: Breakdown of the total down time for the PF-AR in FY2020.

In FY2020, we finally updated the injection section, replacing a septum magnet and aged beam ducts with a cooling water leak [1]. As shown in Fig. 5, the new septum magnet was installed in the atmosphere. The injection beam passes through a thin beam duct made of Inconel inserted between the poles of the septum magnet and is injected into the storage ring through an air gap. The beam duct of the storage ring is made of aluminum alloy, and the cooling water path was installed on the atmospheric side to avoid the risk of leakage in the future.

In the reconstruction, the injection scheme was also changed to reduce the distance between the injection beam and the kicker bump orbit from 15 mm to 9.85 mm. This enabled injection with a smaller initial amplitude for the injected beam. We are trying to improve the injection efficiency and minimize the stored beam disturbance at the top-up injection.

For the PF-AR, detailed operation statistics and the number of failures from FY2011 to FY2020 are listed in Table 4. A breakdown of the total downtime in FY2020 is shown in Fig. 6.

As already explained for the PF ring, due to the pulse bend failure that occurred at the end of the fiscal year, injection to the PF-AR was also disturbed for several days and the user time was cancelled on March 30. Therefore, the total failure time of the PF-AR was more than double that of the last year. On the other hand, the number of failures during the year was as low as in FY2019. The MTBF of the PF-AR was only about 50 hours until FY2018. This is mainly because the PF-AR required acceleration from 3 GeV to 6.5 GeV after accumulation instead of full-energy injection. Another reason was the frequent lifetime drops caused by dust trapping. In FY2018, full-energy injection was enabled by constructing the direct beam transport line from the injector linac, and it became customary to keep the stored current constant by top-up injection. We can clearly see the effect of these improvements in the operation statistics. The number of failures was significantly reduced in FY2019 and FY2020, and the MTBF became equal to or longer than that of the PF-ring.

One topic regarding the PF-AR is the construction of a test beamline, which is planned to deliver GeV-range electrons for developing detectors for particle physics. The Fuji test beamline in the KEKB Factory was shut down, so there is high demand from the physics community. The test beamline is scheduled to start service in 2021.

The test-beam laboratory will be constructed in the south experimental hall of the PF-AR. The overall layout is shown in Fig. 7. A thin wire target is placed just upstream of a bending magnet of the PF-AR, where the γ -rays produced by collisions with stored beams are converted into electron-positron pairs by a copper converter installed at the end of the bending magnet chamber. The beamline, which leads electrons to the test beam area, has a simple configuration with one bending magnet and seven quadrupole magnets placed at the same level in front of and behind the bending magnet, aiming to transport electrons with minimal loss. A new mezzanine floor has been constructed in the south experimental hall to house the beam shutter, quadrupole magnets, and the laboratory space.

We plan to use the test beamlines and conduct synchrotron radiation experiments simultaneously, rather than by time-sharing. In order to minimize the disturbance to synchrotron radiation experiments, a thin wire will be inserted at a distance of 5σ outward from the beam orbit, where σ is the horizontal beam size of the stored beam. The beam halo will interrupt with the thin wire. With this arrangement, it has been confirmed by simulation that several thousand energy-selected electrons will be available at the test-beam laboratory. The only effect on the synchrotron radiation use is estimated to be a decrease of the beam lifetime by 10%, which top-up injection can cover without difficulty.

REFERENCES

- [1] C. Mitsuda, K. Harada, N. Higashi, T. Honda, Y. Kobayashi, H. Miyauchi, S. Nagahashi, N. Nakamura, T. Nogami, T. Obina, M. Tadano, R. Takai, H. Takaki, Y. Tanimoto, T. Uchiyama and A. Ueda, *IPAC'21 MOPAB091* (2021).

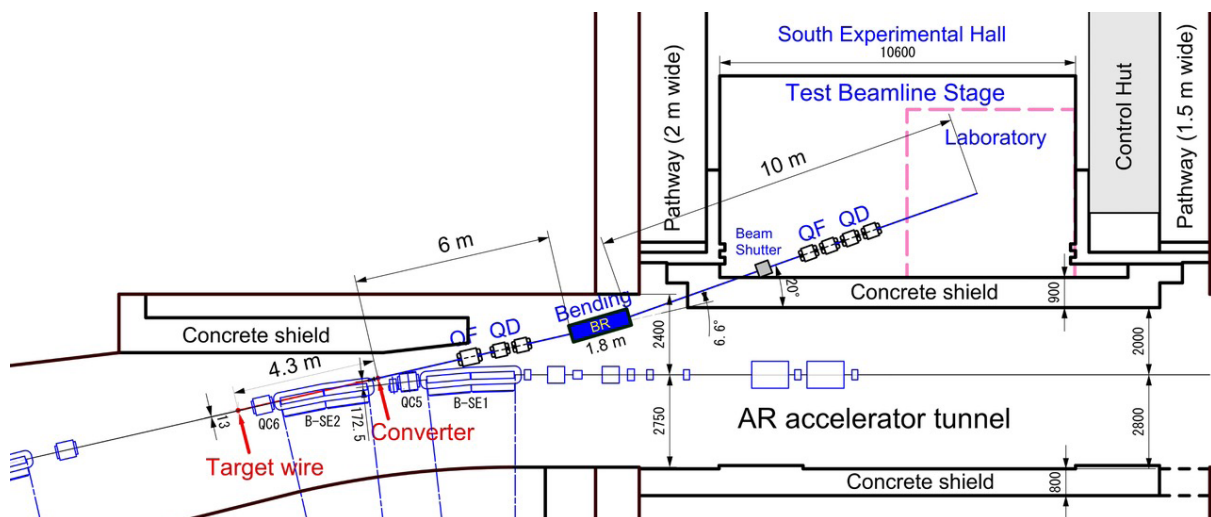


Figure 7: Construction plan of a test beamline at the south experimental hall of the PF-AR.

3. Experimental Stations

Fifty-three experimental stations are in operation at the PF ring, PF-AR and slow positron facility (SPF), as shown in **Figs. 8, 9** and **10**. Thirty-five stations are dedicated to research using hard X-rays, 14 stations

for studies in the VUV and soft X-ray energy regions, and 4 stations for studies using slow positrons. **Tables 5, 6** and **7** summarize the areas of research being carried out at the experimental stations at the PF ring, PF-AR and SPF.

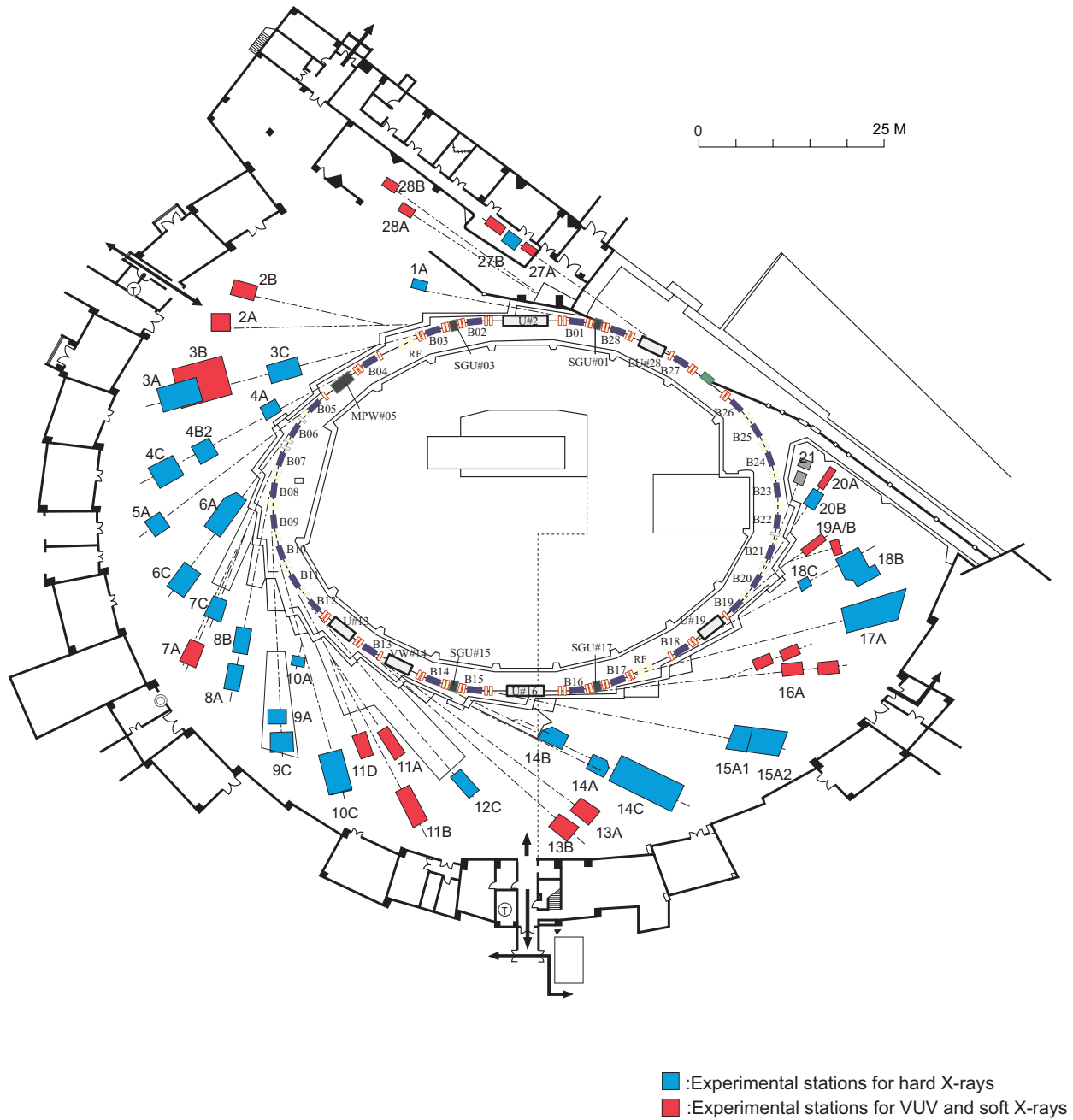


Figure 8: Plan view of the PF experimental hall, showing hard X-ray experimental stations (blue), and VUV and soft X-ray experimental stations (red).

Table 5: List of the experimental stations available for users at the PF ring.

Experimental Station		Person in Charge
BL-1 A	(Short Gap Undulator) Macromolecular crystallography	N. Matsugaki
BL-2 A B	(Variable Polarization Undulator for VUV and planer undulator for SX) High-resolution VUV-SX beamline for angle-resolved photoemission spectroscopy High-resolution VUV-SX spectroscopies	K. Horiba K. Horiba
BL-3 A B C	(A: Short Gap Undulator) X-ray diffraction for material structural science VUV and soft X-ray spectroscopy (♠) Characterization of X-ray optical elements/White X-ray magnetic diffraction	H. Nakao K. Edamoto [Rikkyo Univ.], J. Yoshinobu [The Univ. of Tokyo], K. Mase K. Hirano
BL-4 A B2 C	Trace element analysis, X-ray microprobe (♠) High resolution powder diffraction (♠) X-ray diffraction for material structural science	M. Uo [Tokyo Medical and Dental Univ.], M. Kimura, Y. Niwa H. Uekusa [Tokyo Tech.], H. Nakao H. Nakao
BL-5 A	(Multipole Wiggler) Macromolecular crystallography	N. Matsugaki
BL-6 A C	Small-angle X-ray scattering X-ray diffraction and spectroscopy (♠)	N. Igarashi N. Happo [Hiroshima City Univ.], H. Nakao
BL-7 A C	Soft X-ray spectroscopy (♦) X-ray spectroscopy and diffraction	J. Okabayashi [RCS, The Univ. of Tokyo], K. Amemiya H. Sugiyama
BL-8 A B	Weissenberg camera for powder/Single-crystal measurements under extreme conditions Weissenberg camera for powder/Single-crystal measurements under extreme conditions	H. Sagayama H. Sagayama
BL-9 A C	XAFS XAFS	H. Abe H. Abe
BL-10 A C	X-ray diffraction and scattering (♠) Small-angle X-ray Scattering	A. Yoshiasa [Kumamoto Univ.], R. Kumai N. Shimizu
BL-11 A B D	Soft X-ray spectroscopy Soft X-ray spectroscopy Characterization of optical elements used in the VSX region	Y. Kitajima Y. Kitajima K. Mase
BL-12 C	XAFS	H. Nitani

Experimental Station		Person in Charge
BL-13 A/B	(Variable Polarization Undulator) VUV and soft X-ray spectroscopies with circular and linear polarization	K. Mase
BL-14 A B C	(Vertical Wiggler) Crystal structure analysis and detector development High-precision X-ray optics Medical applications and general purpose (X-ray)	S. Kishimoto K. Hirano K. Hirano
BL-15 A1 A2	(Short Gap Undulator) Semi-microbeam XAFS High brilliance small-angle X-ray scattering	Y. Takeichi H. Takagi
BL-16 A	(Variable Polarization Undulator) Soft X-ray spectroscopies with circular and linear polarization	K. Amemiya
BL-17 A	(Short Gap Undulator) Macromolecular crystallography	Y. Yamada
BL-18 B C	Multipurpose monochromatic hard X-ray station (◆) High pressure X-ray powder diffraction (DAC) (♠)	P. Saha [JNCASR], R. Kumai H. Kagi [The Univ. of Tokyo], N. Funamori
BL-19 A/B	(Variable Polarization Undulator) Soft X-ray microscopy and spectroscopy	K. Ono
BL-20 A B	VUV spectroscopy (◇) White & monochromatic X-ray topography and X-ray diffraction experiment	M. Kitajima [Tokyo Tech], J. Adachi H. Sugiyama
BL-27 A B	(Beamline for radioactive samples) Radiation biology, soft X-ray photoelectron spectroscopy Radiation biology, XAFS	A. Yokoya [QST], Y. Okamoto [JAEA], N. Usami A. Yokoya [QST], Y. Okamoto [JAEA], N. Usami
BL-28 A B	(Variable Polarization Undulator) High-resolution angle-resolved photoemission spectroscopy with circular and linear polarization High-resolution VUV spectroscopies with circular and linear polarization	K. Horiba K. Horiba

- ♠ User group operated beamline
◆ External beamline
◇ Operated by University

RCS: Research Center for Spectrochemistry, the University of Tokyo
JNCASR: Jawaharlal Nehru Centre for Advanced Scientific Research

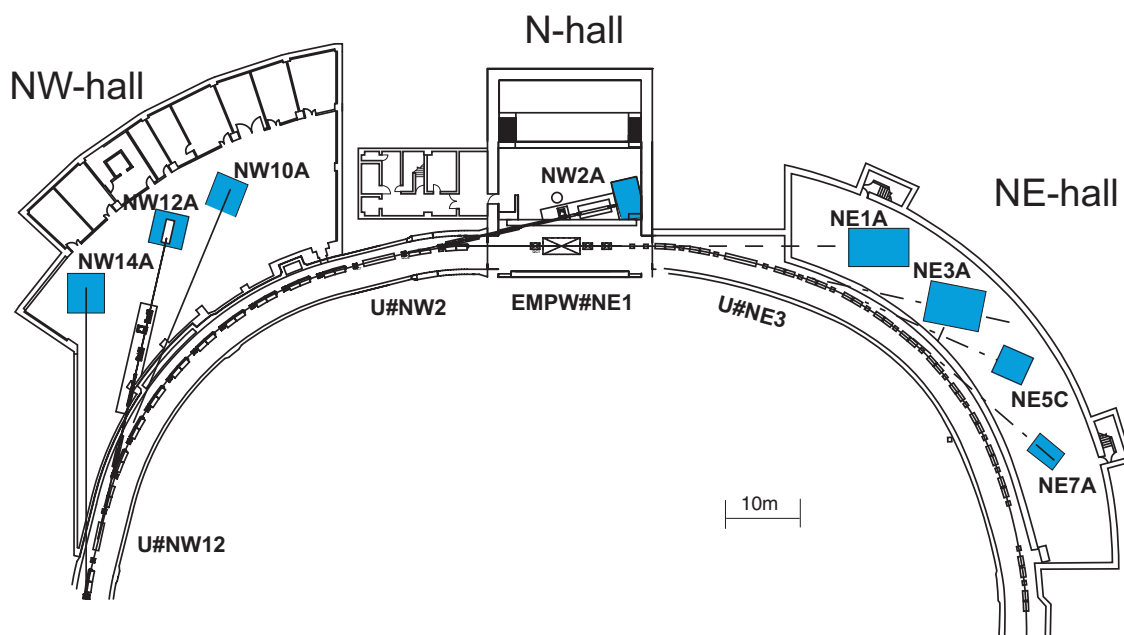


Figure 9: Plan view of the beamlines in the PF-AR north-east, north, and north-west experimental halls.

Table 6: List of the experimental stations at PF-AR.

Experimental Station		Person in Charge
AR-NE1	(Multipole Wiggler)	N. Funamori
A	Laser-heating high pressure X-ray diffraction and nuclear resonant scattering (DAC)	
AR-NE3	(In-vacuum Undulator)	Y. Yamada
A	Macromolecular crystallography	
AR-NE5		N. Funamori
C	High pressure and high temperature X-ray diffraction (MAX-80)	
AR-NE7		K. Hirano, Kubo [Kyusyu Univ.]
A	High pressure and high temperature X-ray diffraction (MAX-III) (♥), X-ray imaging	
AR-NW2	(In-vacuum Type Tapered Undulator)	Y. Niwa
A	Time-resolved Dispersive XAFS/XAFS/X-ray Diffraction	
AR-NW10		H. Nitani
A	XAFS	
AR-NW12	(In-vacuum Type Tapered Undulator)	M. Hikita
A	Macromolecular crystallography	
AR-NW14	(In-vacuum Undulator)	S. Nozawa
A	Time-resolved X-ray diffraction, scattering and absorption	

♥ User group operated Experimental equipment operated by user groups

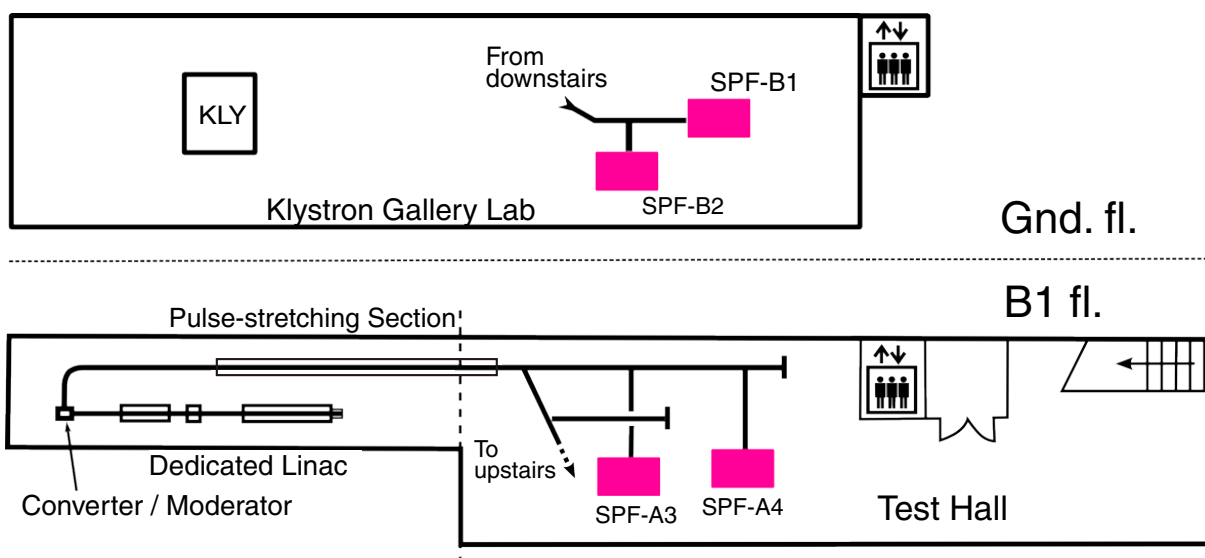


Figure 10: View of the beamlines in the Slow Positron Facility.

Table 7: List of the experimental stations in the Slow Positron Facility.

Experimental Station		Person in Charge
SPF-A3	Total-reflection high-energy positron diffraction	K. Wada
SPF-A4	Low-energy positron diffraction	K. Wada
SPF-B1	General purpose (Positronium laser cooling)	K. Wada
SPF-B2	Positronium time-of-flight	K. Wada

4. Summary of User Proposals

The Photon Factory accepts experimental proposals submitted by researchers mainly at universities and research institutes inside and outside Japan. The PF Program Advisory Committee (PF-PAC) reviews the proposals, and the Advisory Committee for the Institute of Materials Structure Science approves those that are favorably recommended. The number of accepted proposals over the period 2009–2020 is shown in **Table 8**, where S1/S2, U, G, P, and MP denote Special, Urgent, General, Preliminary, and Multi-Probe proposals, respectively. Category T is a proposal for supporting researches by PhD students. Category MP is a proposal in which at least two of the four beams, synchrotron radiation at the PF, slow positron beam at Slow Positron Facility, and neutron and muon beams at the Materials and Life Science Experimental Facility (MLF) in J-PARC, are required to be used, as a multi-probe experiment.

Category C is a proposal for collaboration between KEK and a research institute including a private company. Category I is a non-proprietary proposal for the integrated promotion of social system reform and re-

search and development, supported by the Ministry of Education, Culture, Sports, Science and Technology (from 2009 to 2015).

Category V is a non-proprietary grant-aided proposal that has already been reviewed and approved for a research grant; beam time for proposals in this category is allocated with high priority, and applicants are required to pay the stipulated fees for the beam time. Category Y is a proprietary proposal; applicants are required to pay the stipulated fees for the beam time. Category Y and Category L are proprietary proposals for general applicants and beginner applicants, respectively. Those applicants are required to pay the stipulated fees for the beam time.

The number of current G-type proposals each year has exceeded 700 for the past few years. In addition to these proposals, 53 projects in the BINDS program (Basis for Supporting Innovative Drug Discovery and Life Science Research) were performed at the PF in FY2020. A full list of the proposals effective in FY2020 and their scientific output can be found in the Photon Factory Activity Report (<https://www2.kek.jp/imss/pf/science/publ/acrpubl.html>).

Table 8: Number of proposals accepted for the period 2009–2020.

category	FY-2009	2010	2011	2012	2013	2014	2015	2016	2017	2018	2019	2020
S1	0	0	0	0	0	0	0	0	0	1	0	0
S2	6	3	2	4	5	4	7	6	1	6	3	2
U	2	2	0	4	1	0	1	0	0	0	0	2
G	397	407	415	454	447	407	361	372	392	321	350	297
P	14	16	11	18	18	5	16	10	16	16	18	9
T						6	4	3	3	2	3	0
MP							3	0	0	1	-	-
C	12	15	19	20	20	25	24	19	21	21	22	18
I	9	17	13	17	13	16	11	-	-	-	-	-
V				1	2	2	2	4	4	10	7	8
Y	29	31	30	30	41	22	33	39	30	39	37	28
L									3	7	15	12

S-type proposals consist of two categories, S1 and S2. S1 proposals are self-contained projects of excellent scientific quality, and include projects such as the construction and improvement of beamlines and experimental stations which will be available for general users after the completion of the project. S2 proposals are superior-grade projects that require the full use of synchrotron radiation or long-term beam time. Proposals are categorized into five scientific disciplines, and reviewed by the five subcommittees of PF-PAC: 1) electronic structure, 2) structural science, 3) chemistry and materials, 4) life science I (protein crystallography), and 5) life science II (including soft matter science). **Figure 11** shows the distribution by research field of the proposals accepted by the subcommittees in FY2020.

The number of users for all types of proposals is about 2,000. About 16% of the proposals are conducted by new spokespersons, indicating that the Photon Factory is open to public academic users. **Figure 12** shows the distribution of users by institution and their positions. Over three-quarters of the users belong to universities. About two-thirds of the university users are graduate and undergraduate students, clearly showing the important role that the Photon Factory plays in both research

and education. The geographical distribution of the Photon Factory users is shown in **Figs. 13** and **14**, which also indicates the immense contribution of the Photon Factory to research and education throughout Japan. The registered number of papers published in 2020 based on experiments at the PF was 619 at the time of writing (July 1, 2021). In addition, 45 doctoral and 291 master theses have been presented.

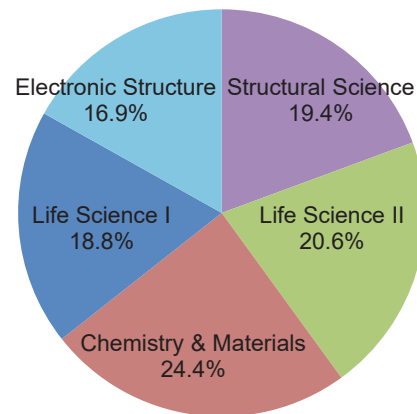


Figure 11: Distribution by scientific field of experimental proposals accepted in FY2020.

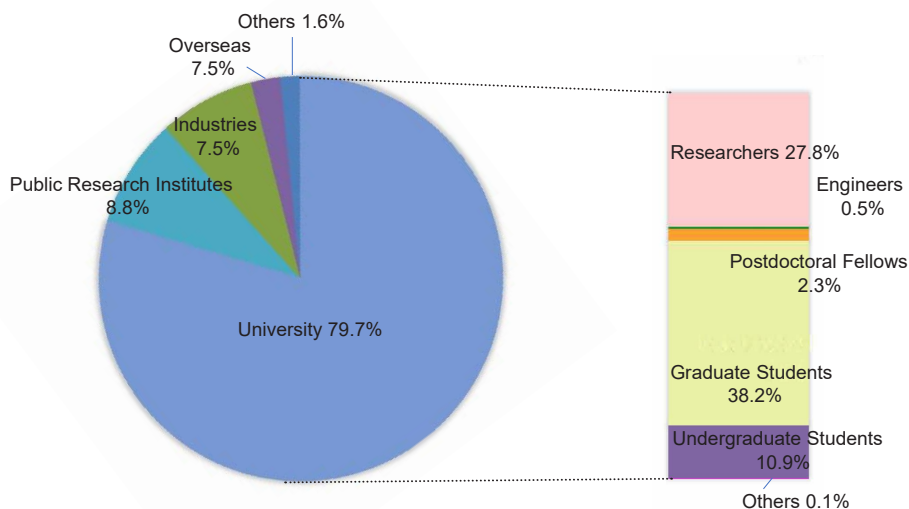


Figure 12: Distribution of users by institution and position.

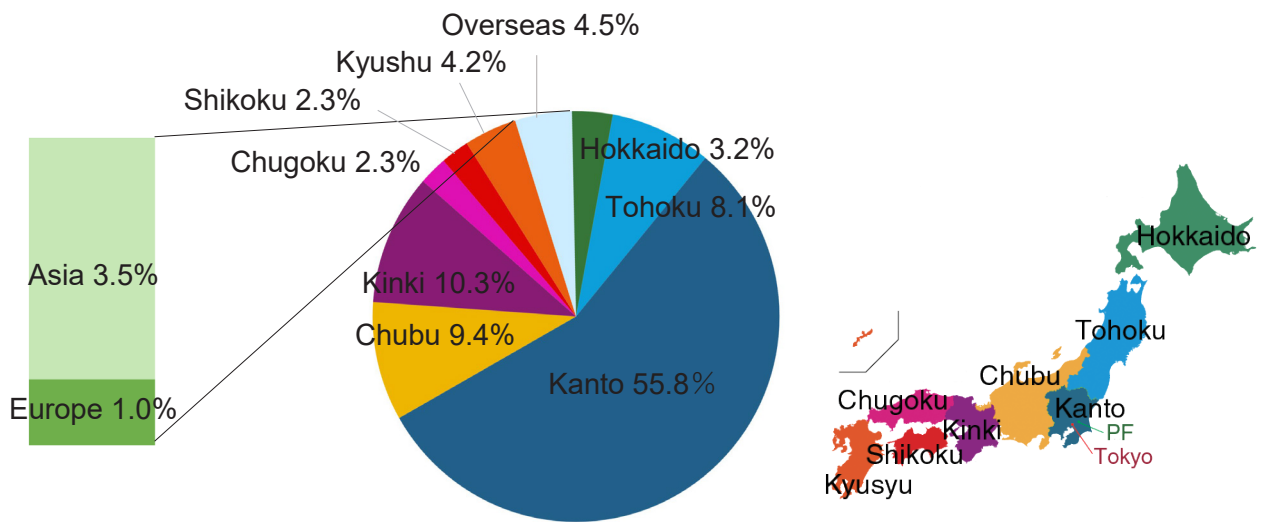


Figure 13: Regional distribution of spokespersons of proposals accepted in FY2020.

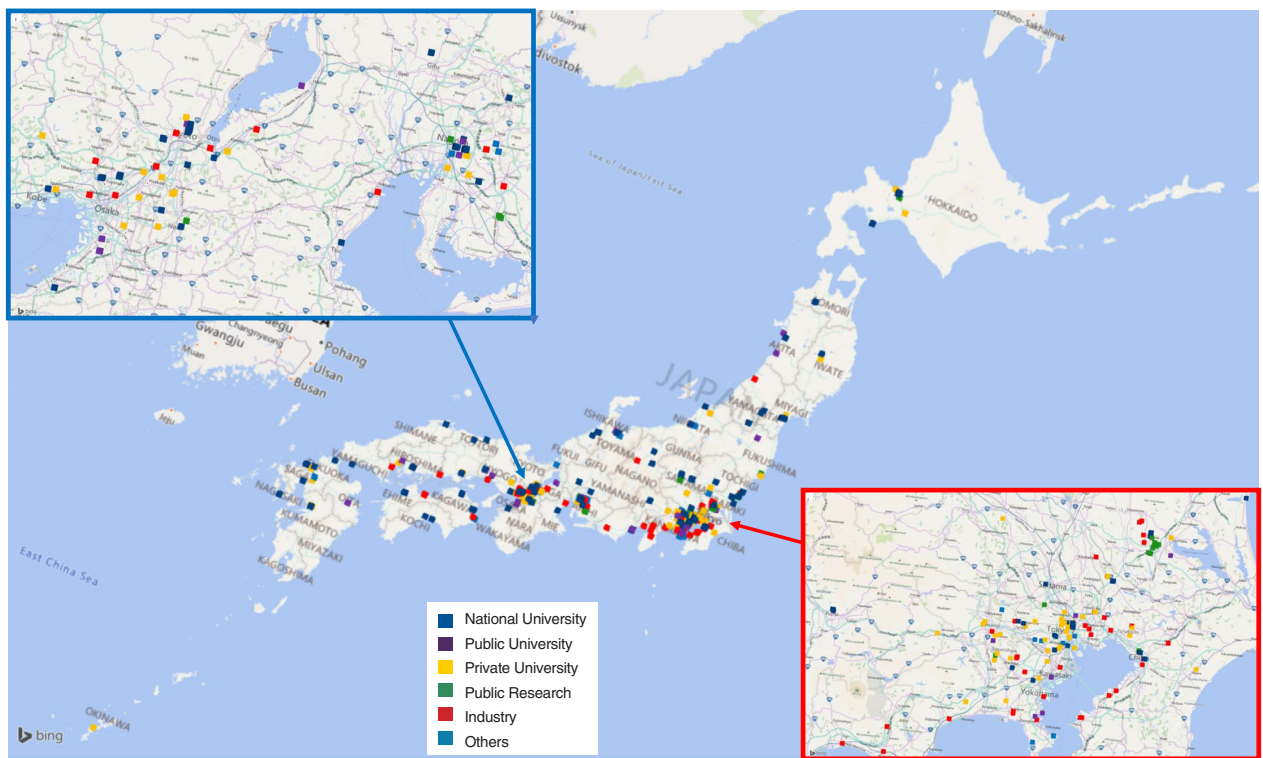


Figure 14: Geographical distribution of Photon Factory users in FY2020 (domestic users only).